

Light Sensitivity Within Areas of Geographic Atrophy Secondary to Age-Related Macular Degeneration

Maximilian Pfau,^{1,2} Leon von der Emde,¹ Chantal Dysli,^{1,3} Sarah Thiele,^{1,2} Philipp T. Möller,^{1,2} Moritz Lindner,⁴ Jennifer Nadal,⁵ Matthias Schmid,⁵ Steffen Schmitz-Valckenberg,^{1,2} Frank G. Holz,^{1,2} and Monika Fleckenstein^{1,2}

¹University of Bonn, Department of Ophthalmology, Bonn, Germany

²GRADE Reading Center, Bonn, Germany

³Department of Ophthalmology and Department of Clinical Research, Inselspital, Bern University Hospital and University of Bern, Bern, Switzerland

⁴The Nuffield Laboratory of Ophthalmology, Sleep and Circadian Neuroscience Institute, Nuffield Department of Clinical Neurosciences, University of Oxford, Oxford, United Kingdom

⁵Institute for Medical Biometry, Informatics and Epidemiology, University Hospital Bonn, Germany

Correspondence: Monika Fleckenstein, Department of Ophthalmology, University of Bonn, Ernst-Abbe-Straße 2, Bonn 53127, Germany; mfleckenstein@web.de.

Submitted: March 27, 2019

Accepted: August 13, 2019

Citation: Pfau M, von der Emde L, Dysli C, et al. Light sensitivity within areas of geographic atrophy secondary to age-related macular degeneration. *Invest Ophthalmol Vis Sci*. 2019;60:3992–4001. <https://doi.org/10.1167/iovs.19-27178>

PURPOSE. To investigate residual sensitivity within geographic atrophy (GA) secondary to age-related macular degeneration.

METHODS. Mesopic and dark-adapted (DA) cyan and red light sensitivity (Goldmann III) were investigated using fundus-controlled perimetry (microperimetry). Test points were placed within GA along an “iso-hull” with a distance of -0.645° to the atrophy boundary. The false-positive response rate was determined with suprathreshold stimuli to the optic disc (Heijl-Krakau method) and used to compute the expected sensitivity measurements for the assumption of absolute scotomata. The outermost visible retinal layer on spectral-domain optical coherence tomography at the location of each test point was determined.

RESULTS. Thirty eyes of 36 patients (75.55 ± 7.93 years; 19 female) from the prospective natural history study Directional Spread in Geographic Atrophy (NCT02051998), with a total of 1380 threshold determinations were analyzed. The measured sensitivities were significantly ($P < 0.01$) higher than the expected values for absolute scotomata (mean \pm standard error of $+6.92 \pm 0.86$ dB for mesopic, $+2.57 \pm 0.56$ dB for DA cyan, and $+4.93 \pm 0.74$ dB for DA red testing). For mesopic testing and DA red testing, the presence of a residual outer nuclear layer had a significant effect on this discrepancy ($P < 0.001$). There was no effect of fixation stability or any other reliability index on this discrepancy.

CONCLUSIONS. Measured sensitivities within the inner junctional zone of GA may not be purely explained by patient-specific false-positive response rates or other reliability indices. The marked influence of the outer retinal configuration on measured sensitivity may be indicative of residual cone function within GA at the inner junctional zone.

Keywords: microperimetry, scotopic perimetry, geographic atrophy, age-related macular degeneration, AMD, GA

Geographic atrophy (GA) secondary to age-related macular degeneration (AMD), constitutes one of the major causes of legal blindness in industrial countries.^{1–3} Hereby, the term GA traditionally refers to complete atrophy of the retinal pigment epithelium (RPE) as seen on funduscopic examination or color fundus photography (CFP).⁴ Using fundus autofluorescence (FAF) confocal scanning laser ophthalmoscopy (cSLO) imaging, areas of GA may be accurately detected and quantified, since the loss of RPE and its inherent fluorophores in GA correlates with well-defined areas of decreased autofluorescence.^{5,6} Enlargement of atrophy as detected by FAF is accepted as a validated anatomical end point by the U.S. Food and Drug Administration.⁷

However, in vivo spectral-domain optical coherence tomography (SD-OCT) imaging as well as histologic data reveals a more complex architecture of the junctional zone of GA, whereby the spatial sequence of degenerative changes may be

viewed as a surrogate for time and disease progression.^{8–11} Briefly, three putative boundaries are visible: (1) loss of the RPE component of the outer retinal band 4,^{12,13} (2) descent of the external limiting membrane (ELM) toward Bruch’s membrane (BrM),¹⁴ and (3) descent of the outer nuclear layer/outer plexiform layer (ONL/OPL) boundary toward BrM.^{8,15} This third boundary delineates areas of complete RPE and outer retinal atrophy (cRORA).¹⁶ Yet, the third boundary may also be absent with residual Henle’s fiber layer and outer nuclear layer (HFL+ONL) bridging the entire area of RPE atrophy.¹⁵ Based on histologic data, the ELM descent has been shown to delimit marked gliosis and near-total photoreceptor degeneration, suggesting that the residual (bridging) HFL+ONL in areas of atrophy has no significant functional relevance.^{9–11} However, residual cone photoreceptor nuclei have also been described on the atrophic side of the ELM descent (e.g., figure 2C in Ref. 10).^{10,11} Moreover, photoreceptors may be present in the



junctional zone in the form of so-called outer retinal tubulations (ORTs).^{17,18} These tubular arrangements of photoreceptors have been observed to evolve through progressive scrolling of photoreceptors at the site of the ELM descent and are readily identifiable on SD-OCT images based on their hyperreflective boundary (compare schematic representation of ORT development in figure 8 in Ref. 18). To date, the precise functional implications of both, residual HFL+ONL and/or ORTs, within GA are unknown.

The aim of this study was to explore the possibility of residual sensitivity within the inner junctional zone of GA (atrophic side of GA boundary) and to determine the functional implications of residual HFL+ONL and/or ORTs using fundus-controlled perimetry. Given that clinical end points ought to represent close correlates of function, this study constitutes a prerequisite to define the “functional boundary” of GA in relation to clinical imaging.

METHODS

Patients

Patients were recruited in the context of the noninterventional prospective natural history study Directional Spread in Geographic Atrophy (DSGA, NCT02051998) at the Department of Ophthalmology at the University Hospital in Bonn, Germany.^{19,20} Briefly, patients had to be at least 55 years of age and exhibit unifocal or multifocal GA, defined as any sharply demarcated round or oval-shaped lesion of at least 0.05 mm² in area, and have clearly reduced FAF in the context of AMD-associated changes (i.e., drusen and pigment abnormalities).¹⁹ Exclusion criteria included the presence of other retinal diseases such as diabetic retinopathy or retinal dystrophy, as well as a history of laser photocoagulation or retinal surgery, any signs of active or regressed exudation (e.g., hemorrhages, exudates, fibrous scarring), as well as refractive errors >5.00 diopters spherical equivalent or >2.50 diopters astigmatism in the study eye. This study adhered to the tenets of the Declaration of Helsinki and was approved by the institutional review board (Institutional Review Board of the University of Bonn, approval ID: 197/12). Written informed consent was obtained from each participant after explanation of the study's nature and possible consequences of participation. In a previous publication, we analyzed in a subset ($n = 25$) of the current study cohort the retinal sensitivity in the junctional zone of atrophy, that is, at retinal locations away from the GA boundary.²¹

Imaging

Following pupil dilatation with 0.5% tropicamide and 2.5% phenylephrine, patients underwent 30° × 30° fundus autofluorescence imaging (λ excitation 488 nm, λ emission 500–700 nm), 30° × 30° infrared reflectance (λ 815 nm) imaging, and 30° × 25° SD-OCT imaging (121 B-scans) (Spectralis HRA-OCT2; Heidelberg Engineering, Heidelberg, Germany). Hereby, the automatic real-time tracking (ART; i.e., number of averaged frames per B-scan) was set to 25 to provide high image resolution at the junctional zone.²² Areas of GA were semiautomatically annotated using the software (RegionFinder; Heidelberg Engineering) based on fundus autofluorescence and infrared reflectance images as previously described.^{6,23}

Patient-Tailored Perimetry Grids

The method for generation of the patient-tailored perimetry grids has previously been described in detail.²¹ Briefly, patient-tailored fundus-controlled perimetry (FCP) grids were gener-

ated using customized software developed in the MATLAB software environment (MathWorks, Natick, MA, USA). The software traced the boundaries of annotated GA lesions and placed test points along “iso-hulls” surrounding the GA boundary. For the analysis shown here, only test points within GA (i.e., on the −0.645° iso-hull, [187 μ m in an emmetropic eye]) were considered. This distance was chosen to provide sufficient distance to the GA boundary (i.e., distance of 0.43° [equal to 1 Goldmann III stimulus] after consideration of the area of the stimulus itself), while still coinciding occasionally with residual HFL+ONL. These grids were subsequently saved as XML file and imported in the S-MAIA device (CenterVue, Padova, Italy).

Fundus-Controlled Perimetry

FCP (microperimetry) was performed with the S-MAIA device as previously outlined.^{21,24–26} A brief mesopic examination was performed in patients with no prior perimetry or FCP experience, followed by three different FCP examinations with a retest for each (i.e., total of six tests) using the identical patient-tailored grid: duplicate mesopic (achromatic stimuli, 400–800 nm) FCP as well as duplicate dark-adapted cyan (505 nm) and duplicate dark-adapted red (627 nm) testing. Prior to dark-adapted testing, patients underwent 35 minutes of dark adaption (light level < 0.1 lux). This technique allows differentiation between rod and cone mediation through analysis of the dark-adapted cyan-red sensitivity difference (described in detail in Ref. 29).^{27–29} The conversion of radiant energy into luminous energy is based on the standard scotopic luminosity function for the S-MAIA device. Accordingly, a pointwise dark-adapted cyan-red sensitivity difference of 0 dB would indicate rod-mediation of both stimuli. A pointwise dark-adapted cyan-red sensitivity difference, which is significantly lower than 0 dB (i.e., negative values) would indicate cone mediation of the red stimulus.²⁹ The FCP grid position was adjusted slightly using the “Change grid position” function of the S-MAIA if the preferred retinal locus differed between the Spectralis and S-MAIA examination. For both mesopic and dark-adapted cyan examinations, the follow-up mode was used for the second examination. For dark-adapted red testing, the follow-up mode was not used for the second examination as it was not available at the time of the study. All tests were performed with the preset 4-2-dB staircase strategy with a stimulus size of 0.43° (Goldmann III).

Image Grading

For all analyses, the data of left eyes were flipped horizontally. The perimetry data of the S-MAIA was registered to the SD-OCT data (subretinal en face image) using vascular bifurcations as landmarks in ImageJ software (<http://imagej.nih.gov/ij/>; provided in the public domain by the National Institutes of Health, Bethesda, MD, USA).²¹ Based on the registration, the central A-scan of each stimulus location was identified and labeled. Two independent graders (MP and MF) annotated these specific locations for the outermost visible layer internal to Bruch's membrane, choosing from HFL+ONL, ORT, OPL/inner nuclear layer (INL). In case of discrepancies, the final decision was made through joint image reevaluation.

Statistical Analyses

Statistical analyses were performed using the software environment R and the add-on package lme4. Visual acuity measurements (Snellen fractions) were converted to the base-10 logarithm of the minimum angle of resolution (logMAR). To quantify the retest reliability (in consideration

TABLE 1. Patient Characteristics

Characteristic	Value
Patients, no.	36 (19 female, 17 male)
Age, y, mean \pm SD (range)	75.55 \pm 7.93 (58.1–89.7)
Visual acuity, logMAR, mean \pm SD	0.51 \pm 0.39
Lesion size, mm ² , mean \pm SD	5.27 \pm 4.44
Number of test points within atrophy (i.e., -0.645° iso-hull) per eye, mean \pm SD	6.4 \pm 2.7

of the nonparametric distribution of the test-retest differences), we calculate the percentages of the absolute test-retest differences (0 dB, <2 dB, <4 dB, and <6 dB) per patient and examination type and summarized these.³⁰

To test whether the measured sensitivities exceed the expectation for the assumption of an absolute scotoma, a simulation model was established (Supplementary Fig. S1). Hereby, we considered the device-specific staircase strategy (4-2), the point-specific initial testing brightness, and the patient-specific rate of false-positive responses to a suprathreshold stimulus presented to the patient's blind spot (i.e., Heijl-Krakau method) during the examination.³¹ The expected values were derived by simulating the staircase procedure 10,000 times for each test point, with the false-positive response rate serving as probability of a pressure event at each step. Furthermore, the 95th sensitivity percentile for each test point was saved. Sensitivity measurements above this percentile may be considered as unlikely under the assumption of an absolute scotoma. The frequencies of observed measurements that deviated significantly from the expected value (i.e., probability < 0.05) were summarized.

To identify variables that may be associated with a discrepancy between measured and expected sensitivities, mixed-effects models that fully accounted for the hierarchical structure of data (i.e., test points nested in eye) were applied. First, we analyzed whether the discrepancy between measured and expected values differed significantly from zero for all three types of testing. Second, we aimed to identify the source of the sensitivity measurements (inaccurate responses or fatigue versus genuine retinal sensitivity). For this, the effect size on this sensitivity discrepancy (measurement versus expected value used as outcome variable in linear mixed-effects modeling) was investigated for predictors pointing toward (1) inaccurate responses or fatigue (age, examination

duration, false-positive response rate for catch trials [Heijl-Krakau method], wrong pressure event rate [false-positive responses outside of the response window of the device],³² initial testing brightness), (2) or toward inaccurate stimulus projection due to insufficient fundus tracking (bivariate contour ellipse area), (3) or toward genuine retinal sensitivity (outermost visible retinal layer). For dark-adapted cyan testing, test points colocalizing to the rod-free zone (i.e., test points with an eccentricity <1°, $n = 6$) were removed from the analysis, since no rod mediation in this region would be expected.³³ Post hoc comparisons (Tukey contrasts) were used to compare the effect of the respective outermost layer on sensitivity.

RESULTS

Cohort Characteristics

A total of 36 eyes of 36 patients with GA secondary to AMD (age [mean \pm SD] 75.6 \pm 7.9 years [range, 58.1–89.7 years]) with a mean visual acuity of 0.51 \pm 0.39 logMAR (approximately 20/40 Snellen equivalent) were included in the study (Table 1). On average, 6.4 \pm 2.7 test points per eye were confined to the -0.645° iso-hull and included in this analysis. For all of these test points, duplicate mesopic, dark-adapted cyan, and red testing sensitivity measurements were available (i.e., total of 1380 threshold measurements within atrophy [3 types of testing \times average of 6.4 test points \times 2 replications \times 36 patients]). In this way, identical values for the test and retest were obtained for (median, interquartile range [IQR]) 42.9% (24.3%–67.5%) of all test points in mesopic testing and for 69% (46.9%–100%) and 57.1% (33.3%–67.9%) of all test points in dark-adapted cyan and dark-adapted red testing, respectively (Table 2).

Configuration of the Inner Junctional Zone

Three major subtypes of the inner junctional zone configuration were observed at the site of functional testing (i.e., -0.645° iso-hull): (1) cRORA at GA boundaries with a close proximity of the ELM descent and OPL/INL descent ($n = 135$ of test points); (2) residual HFL+ONL within areas of RPE atrophy with (partial) bridging of the area of RPE atrophy ($n = 83$); and (3) ORTs ($n = 12$) as shown in Figure 1. Overlay of the FCP test results with the en face SD-OCT allowed for precise pointwise grading of the corresponding configuration of the inner junctional zone (Fig. 2). The interrater reliability for the classification was substantial (unweighted Cohen's κ for two raters = 0.77).

Expected Sensitivity Based on False-Positive Responses Versus Measured Sensitivity

Based on the patient-specific false-positive response rate, the staircase strategy (4-2), and the initial testing brightness of the staircase for each test point, the expected values under the assumption of an absolute scotoma can be simulated for each test point (Supplementary Fig. S1; Fig. 3, left column). Visual inspection as well as linear mixed-effects model analysis confirmed that the measured values were significantly higher as compared to the expected values for absolute scotomata (Fig. 3, right column). The discrepancy between measured and expected values was (mean \pm standard error) +6.92 \pm 0.86 dB for mesopic, +2.57 \pm 0.56 dB for dark-adapted cyan, and +4.93 \pm 0.74 dB for dark-adapted red testing. Furthermore, the percentage of unlikely measurements (i.e., pointwise measurements with a probability of $P < 0.05$ for the

TABLE 2. Test-Retest Differences for Sensitivity Measurements Within GA

Test Type	Absolute Test-Retest Difference	Cumulative Frequency in Percent (Median [IQR])
Mesopic	No change	42.9 (24.3–67.5)
	≤ 2 dB	57.1 (42.9–77.1)
	≤ 4 dB	66.7 (48.2–77.1)
	≤ 6 dB	69 (50–88.1)
Dark-adapted cyan	No change	69 (46.9–100)
	≤ 2 dB	79.8 (50–100)
	≤ 4 dB	82.6 (54.2–100)
	≤ 6 dB	82.6 (54.2–100)
Dark-adapted red	No change	57.1 (33.3–67.9)
	≤ 2 dB	63.6 (50–87)
	≤ 4 dB	69 (50–93.2)
	≤ 6 dB	71.4 (55.4–93.2)

IQR, interquartile range.

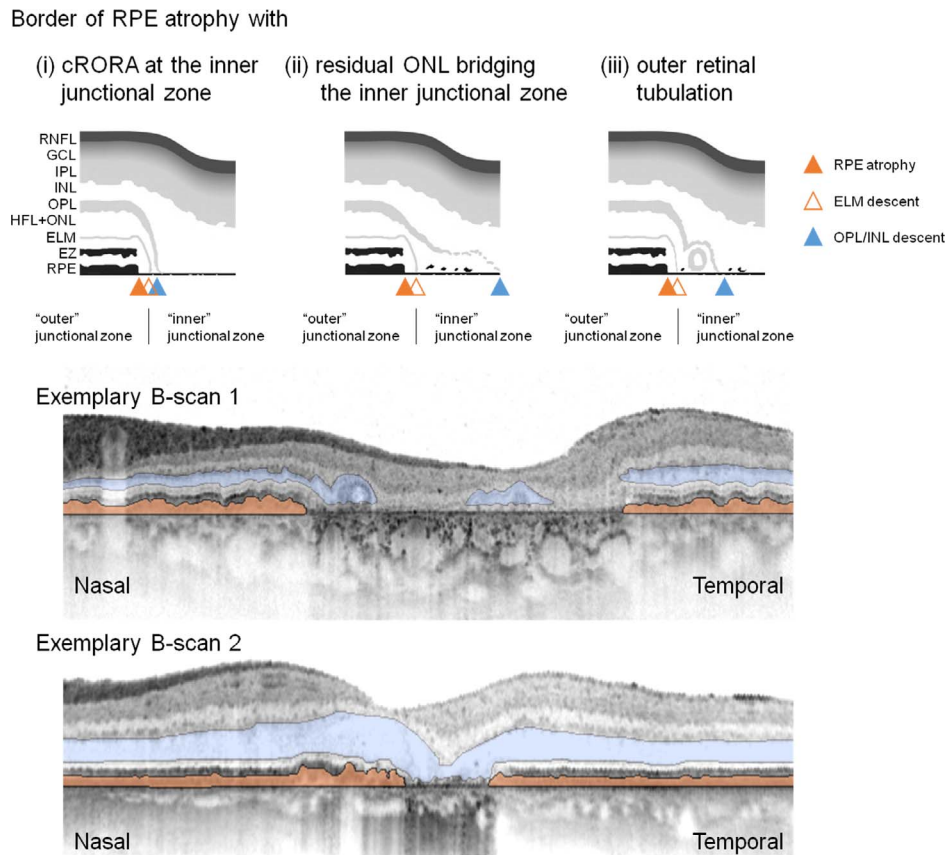


FIGURE 1. Configuration of the inner junctional zone of GA. The *upper row* shows the commonly observable configurations of the inner junctional zone of GA. The boundary may be clinically defined by the atrophy of the RPE as visible in CFP, fundus autofluorescence, and SD-OCT imaging, or by the ELM descent as seen in histologic studies as well as high-resolution SD-OCT imaging. With regard to the atrophy of the HFL+ONL, three configurations may be observed with (1) complete HFL+ONL atrophy (i.e., cRORA), (2) residual HFL+ONL within areas of RPE atrophy (i.e., bridging), or (3) ORTs. The latter two configurations are hallmarked by an increased distance between the ELM descent and the OPL/ONL boundary descent. The SD-OCT B-scans of two patients show an example of an ORT within RPE atrophy (B-scan 1, nasal junctional zone), colocalization of the ELM descent and OPL/ONL boundary descent (B-scan 1, temporal junctional zone), and residual HFL+ONL within RPE atrophy (B-scan 2). SD-OCT layer abbreviations not expanded elsewhere: RNFL, retinal nerve fiber layer; GCL, ganglion cell layer; IPL, inner plexiform layer; EZ, ellipsoid zone. Supplementary Figure S2 shows the same B-scans without the colored overlays.

assumption of absolute scotoma) was (median [IQR]) 34.8% (14.3%–62.8%) for the first mesopic examination, and 35.4% (25%–54.8%) for the second mesopic examination and therefore markedly higher than 5%. For dark-adapted cyan testing, the median percentage of “unlikely” measurements was lower, with 4.5% (0%–37.5%) for the first examination and 0% (0%–27.6%) for the second examination. For dark-adapted red testing, the median percentage of unlikely measurements was 31% (14.3%–64.4%) for the first examination, 25% (0%–50%) for the second examination.

Structure-Function Correlation and Patient Reliability Indices

Visual inspection strongly suggested that the outermost retinal layer influences markedly the discrepancy between measured and expected sensitivity for mesopic testing and dark-adapted red testing (Fig. 4). The same was not observable for dark-adapted cyan testing (Fig. 4). All of the other potential variables such as indicators of inaccurate responses (age, examination duration, false-positive response rate, wrong pressure event rate), indicators of inaccurate stimulus placement due to fixation instability (bivariate contour ellipse area), and characteristics of the staircase procedure (initial testing brightness) exhibited upon visual inspection no marked (linear or

nonlinear) association with the discrepancy between measured and expected sensitivity.

For mesopic testing, the outermost layer in SD-OCT exhibited as a fixed effect a significant effect on this discrepancy (likelihood ratio test, $P < 0.001$, Table 3) as well as the false-positive response rate ($P < 0.001$, Table 3). A post hoc test revealed that the mean discrepancy in measured versus expected sensitivities was significantly higher for test points with residual HFL+ONL versus OPL/INL as the outermost layer in SD-OCT ($+5.96 \pm 0.98$ dB, $P < 0.001$), while the sensitivity discrepancy between test points at ORTs versus OPL/INL differed not significantly ($+2.65 \pm 2.13$ dB, $P = 0.25$).

For dark-adapted red testing, the results were similar. The outermost layer in SD-OCT (likelihood ratio test, $P < 0.001$, Table 3) and the initial testing brightness ($P = 0.0126$), as well as the false-positive response rate ($P < 0.001$), exhibited as fixed effects a significant effect on the discrepancy in measured versus expected sensitivity. The post hoc test revealed, that this discrepancy differed significantly between test points with HFL+ONL versus OPL/INL as the outermost layer in SD-OCT ($+5.19 \pm 0.90$ dB, $P < 0.001$), while no difference was observed for test points at ORTs versus OPL/INL ($+3.32 \pm 1.96$ dB, $P = 0.180$). Test points with HFL+ONL as outermost layer exhibited a significantly reduced pointwise

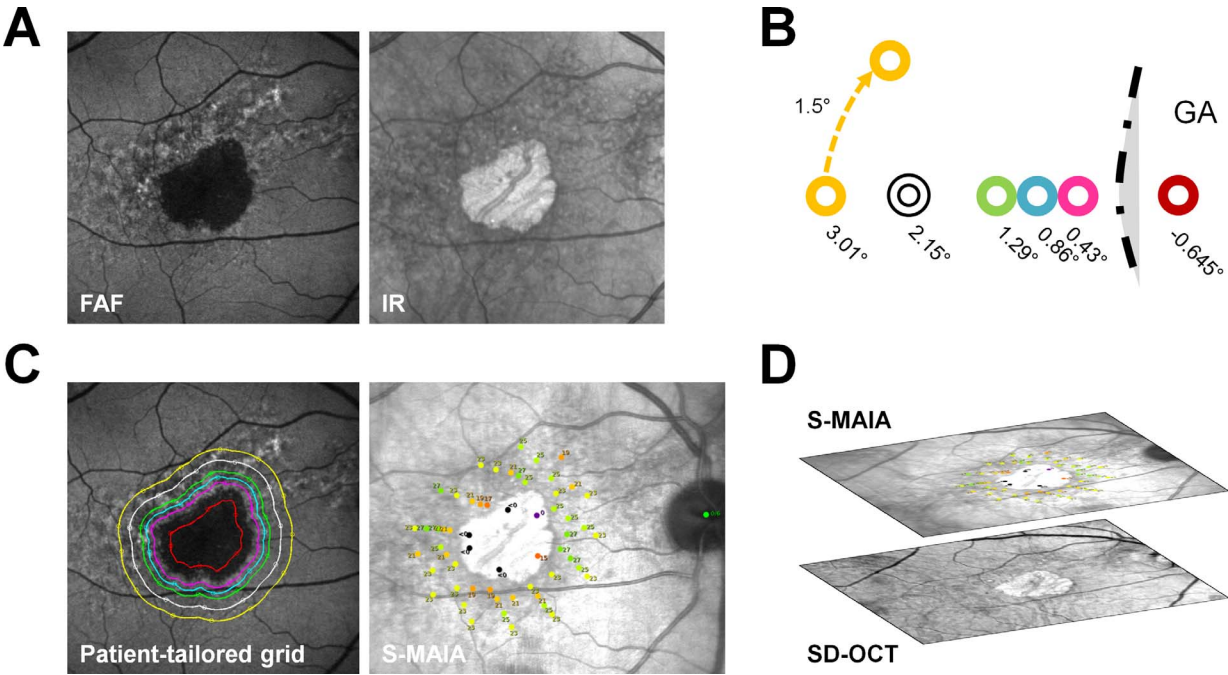


FIGURE 2. Patient-tailored perimetry grids (adapted from Pfau et al.²¹). To probe the retinal function with high spatial resolution at the junctional zone of GA, a novel method was applied. Briefly, multimodal imaging data including FAF and infrared reflectance CSLO imaging (A) was used to automatically generate patient-tailored grids using a custom software. As well as test points along the outer junctional zone, test points at a distance of -0.645° to the GA boundary were placed in the inner junctional zone (compare B and C [red iso-hull]) and evenly spaced along the iso-hull. Panel C shows an exemplary patient-tailored grid that could then be applied for testing in the S-MAIA device. As shown in panel D, registration of the functional data and SD-OCT data was performed based on vessel bifurcations to allow for precise pointwise structure-function correlation.

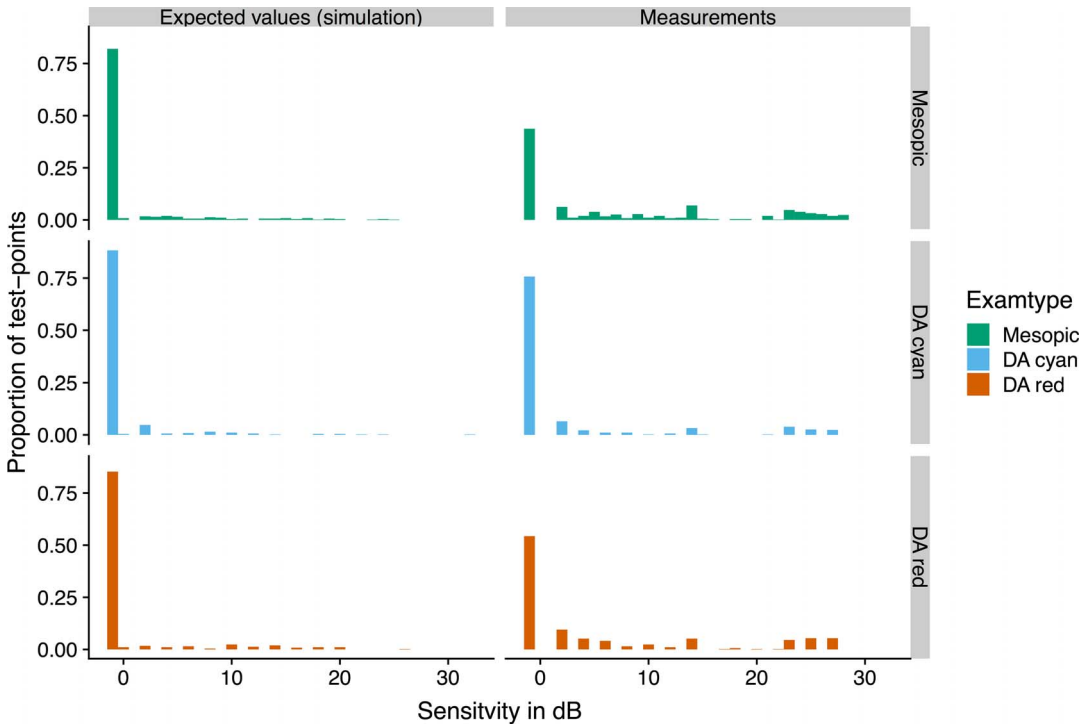


FIGURE 3. Distribution of measured sensitivity within atrophy. This figure shows that the test results are highly skewed, with a large proportion of test values of <0 dB (i.e., zero inflation) for the expected values (based on the patient-specific false-positive response rate, the test point-specific initial testing brightness, as well as the staircase strategy), and for the actual measurements. For mesopic testing and dark-adapted red testing, the actual measurements were markedly higher as compared to the expected values. For dark-adapted cyan testing, the difference between measurements and expected values was much less pronounced.

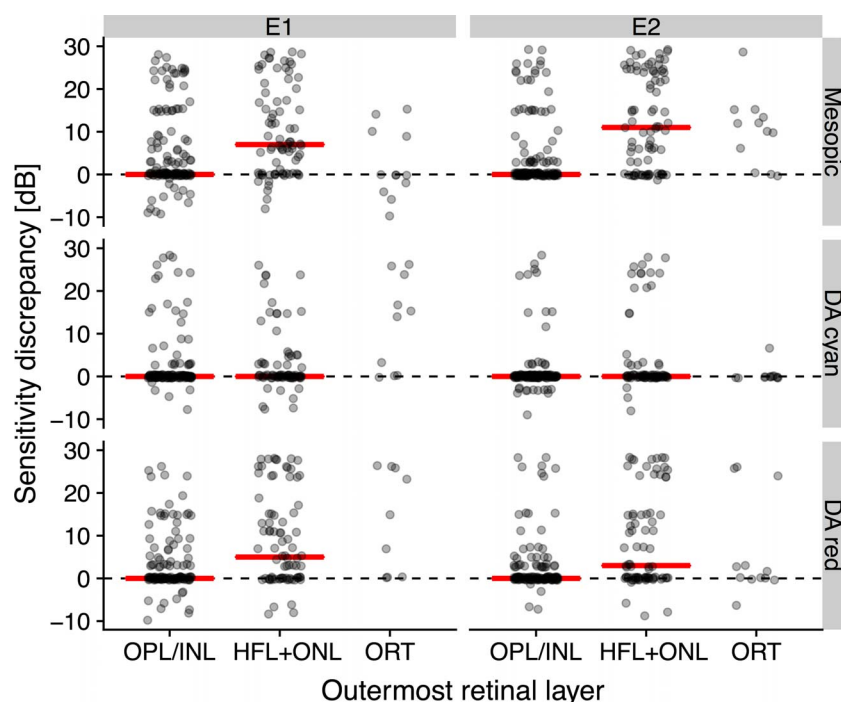


FIGURE 4. Discrepancy between measured and expected sensitivity. The diagram shows the pointwise sensitivity discrepancy between measured and expected sensitivity for all test points in dependence on the outermost intact retinal layer in SD-OCT. The results were plotted separately for the initial examination (E1, *left column*) and the retest (E2, *right column*). To alleviate overplotting, the points were slightly jittered and plotted as semitransparent. The median values (without consideration of the hierarchical structure of the data) are indicated by *red lines*. Please note that test points colocalizing with residual HFL+ONL tended to exhibit higher measurement values than expected for both mesopic and dark-adapted red testing in the first and the second test. In contrast, the results for ORTs were inconsistent. For test points with OPL or INL as outermost layer, the median for the sensitivity discrepancy coincided with 0 dB.

dark-adapted cyan-red sensitivity difference (-5.01 ± 1.07 dB, $P < 0.001$), which indicates that the dark-adapted red sensitivity was cone mediated.²⁹

For dark-adapted cyan testing, neither the outermost layer in SD-OCT nor any other of the probed variables exhibited as a fixed effect a significant association with the discrepancy in measured versus expected sensitivity as indicated by a likelihood ratio test (Table 3).

Two exemplary patients with the schematic staircase results and the corresponding SD-OCT images are provided for clarification of the results (Fig. 5).

DISCUSSION

This study demonstrated that within the inner junctional zone of GA secondary to AMD, light sensitivity might be detected. The expected response distribution for absolute scotomata was considered based on the patient-specific false-positive response rate, the test point-specific initial testing brightness, and the device-specific staircase strategy. The biological plausibility of these findings as well as implications with regard to CFP and FAF as structural outcome measures in GA will be outlined below.

Multiple studies have investigated retinal sensitivity in patients with GA. However, sensitivity within areas of GA was not thoroughly analyzed in the majority of these. Sunness and coworkers³⁴ in 1988 published what we believe to be the first manuscript on FCP in AMD using a custom-built fundus camera stimulator based on a modified Zeiss 30° fundus camera. In this publication, they described that for a patient with GA, no dark-adapted threshold measurements could be obtained in the area of atrophy.³⁴ However, the authors also

described that retinal sensitivity was observed at small areas of atrophy “comparable to the size of drusen,” a manifestation that today would be best described as nascent GA, using the current terminology.³⁴ Using a SLO for FCP, the same group in 1995 reported that a small fraction of test points within GA exhibited sensitivity; yet, the origin of this observation remained unknown. In contrast, sensitivity within atrophy was not reported in the majority of the subsequent publications or only secondarily mentioned without any reference to its source (retinal sensitivity versus false-positive responses).^{35–41} More detailed descriptions of sensitivity measurements within GA were provided by more recent studies reporting that sensitivity measurements may be obtained in areas of GA (as defined by absence of RPE) if the outer retina is partially preserved including so-called nascent GA.^{42–44} However, these studies did not consider the rate of false-positive pressure events, the rate of wrong pressure events, and the fixation stability as potential explanatory variables. In fact, the consideration of these factors is of utmost importance in order to precisely differentiate between true retinal sensitivity and false-positive measurements secondary to “trigger-happy” patients or insufficient fundus tracking (i.e., inaccurate stimulus placement).

In the current analysis, we demonstrated that (1) the mesopic sensitivity measurements within GA are dependent on the false-positive response rate as expected, but that (2) these are also dependent on the outer retinal anatomy with residual HFL+ONL being associated with increased sensitivity measurements. (3) Importantly, the fixation stability had no predictive value in the model, indicating that the sensitivity measurements were not explained by insufficient fundus tracking (i.e., inaccurate stimulus placement in the junctional zone). Moreover, dark-adapted two-color testing revealed that this

TABLE 3. Univariate Analysis

Test Type	Variable	Estimate, dB	Std. Error, dB	P Value
Mesopic	Age, y	0.05	0.11	0.6
	Examination duration, min	−0.24	0.31	0.44
	Fixation stability, log ₁₀ (deg ²)	1.76	1.72	0.32
	Lowermost layer			<0.001
	HFL+ONL vs. OPL/INL	5.91	0.98	
	ORT vs. OPL/INL	2.47	2.13	
	ORT vs. HFL+ONL	−3.44	2.16	
	Wrong pressure event rate, per min	3.5	2.69	0.2
	Initial staircase brightness, dB	0.03	0.06	0.58
	False-positive response rate, % of catch trials	−0.17	0.04	<0.001
Dark-adapted cyan	Age, y	0.02	0.07	0.75
	Examination duration, min	0.31	0.2	0.13
	Fixation stability, log ₁₀ (deg ²)	−0.84	1.44	0.56
	Lowermost layer			0.12
	HFL+ONL vs. OPL/INL	1.02	0.78	
	ORT vs. OPL/INL	3.11	1.69	
	ORT vs. HFL+ONL	2.09	1.71	
	Wrong pressure event rate, per min	0.66	3.13	0.84
	Initial staircase brightness, dB	0.09	0.05	0.09
	False positive response rate, % of catch trials	−0.11	0.03	0.84
Dark-adapted red	Age, y	0.01	0.09	0.95
	Examination duration, min	0.33	0.25	0.19
	Fixation stability, log ₁₀ (deg ²)	0.73	1.8	0.68
	Lowermost layer			<0.001
	HFL+ONL vs. OPL/INL	5.36	0.91	
	ORT vs. OPL/INL	3.49	1.99	
	ORT vs. HFL+ONL	−1.87	2.02	
	Wrong pressure event rate, per min	1.91	3.24	0.56
	Initial staircase brightness, dB	0.15	0.06	0.0126
	False-positive response rate, % of catch trials	−0.27	0.05	<0.001

The table shows the results of the univariate analysis. The estimates represent the effect of the potential prognostic variables on the discrepancy between the measured and expected sensitivity. All mixed-model analyses considered the hierarchical nature of the data (test points nested in eye, repeated measures). *P* values were obtained using a likelihood ratio test. Please note, for mesopic and dark-adapted red testing, the estimates reported in the main text for the lowermost layer were derived from a multivariate model (considering the lowermost layer and false-positive response rate for mesopic testing and the lowermost layer, false-positive response rate, as well as the initial staircase brightness for dark-adapted red testing). Values in bold indicate statistical significance.

residual mesopic sensitivity within GA was reproducible for dark-adapted red testing, but not for dark-adapted cyan testing. This suggests that the measured residual function is most likely cone mediated. Biologically, this appears plausible, given that the cone-specific visual cycle is independent of the RPE, in contrast to the canonical visual cycle required for rod function.⁴⁵ Moreover, this observation is compatible with early histopathologic studies by Curcio and coworkers^{46,47} demonstrating that rod photoreceptor loss exceeds and (spatially) precedes cone photoreceptor loss in late-stage AMD.

With regard to structural imaging, Fleckenstein and coworkers⁸ in 2008 and Bearely et al.¹⁵ in 2009 described qualitatively and quantitatively that the OPL/ONL boundary descent (i.e., the boundary indicating complete HFL+ONL atrophy) is commonly within the boundaries of RPE atrophy or even absent (i.e., HFL+ONL bridging GA) in SD-OCT. Histologic studies suggest that this residual HFL+ONL band within atrophy mostly represent dyslaminated HFL; however, residual photoreceptors in form of ORTs and photoreceptor islands with presence of residual RPE (also termed open ORTs) have also been described.^{10,11,17,48} While ORTs are readily recognizable using SD-OCT, the differentiation between delaminated HFL and photoreceptor islands (without regularly arranged inner and outer segments) is likely not possible using SD-OCT.¹⁷ Both of these entities would be perceived as a hyporeflective OCT band external to the OPL. This may explain the model uncertainty (wide standard error of the

estimate) for the effect of HFL+ONL presence within GA on sensitivity. Potentially, in vivo fluorescence lifetime imaging could have allowed for a differentiation between delaminated HFL and photoreceptor islands (without regularly arranged inner and outer segments).⁴⁹ Previous studies using this technique observed an “intermediate lifetime border” within GA (i.e., inner junctional zone), which is indicative of visual cycle by-products supporting the hypothesis of remnant visual function in these regions.^{50,51} Moreover, histologic studies evidenced, besides the presence of degenerative cone photoreceptor cell bodies and nuclei (compare figure 6 in Ref. 11), opsin redistribution to cone cell bodies, axons, or axon terminals in the setting of AMD, which could explain the herein observed residual sensitivity in spite of the absence of outer segments in SD-OCT.^{52,53}

The current work may also have implications for clinical trials in patients with GA. Firstly, with regard to CFP and FAF as structural end points, it must be recognized that delineation of areas of GA in CFP or as definitely decreased FAF is not exactly homonymous to the area of absolute scotoma.^{7,54} Nevertheless, areas of definitely decreased FAF correspond to deep scotomata even in presence of residual outer retinal layer as compared to the immediately surrounding retina. We have previously shown that the pointwise mesopic sensitivity loss in reference to spatially corresponding normative data of (median) −22.9 dB at −0.645° within RPE atrophy versus (mean) −10.68 dB at +0.43° outside of RPE atrophy is indicative

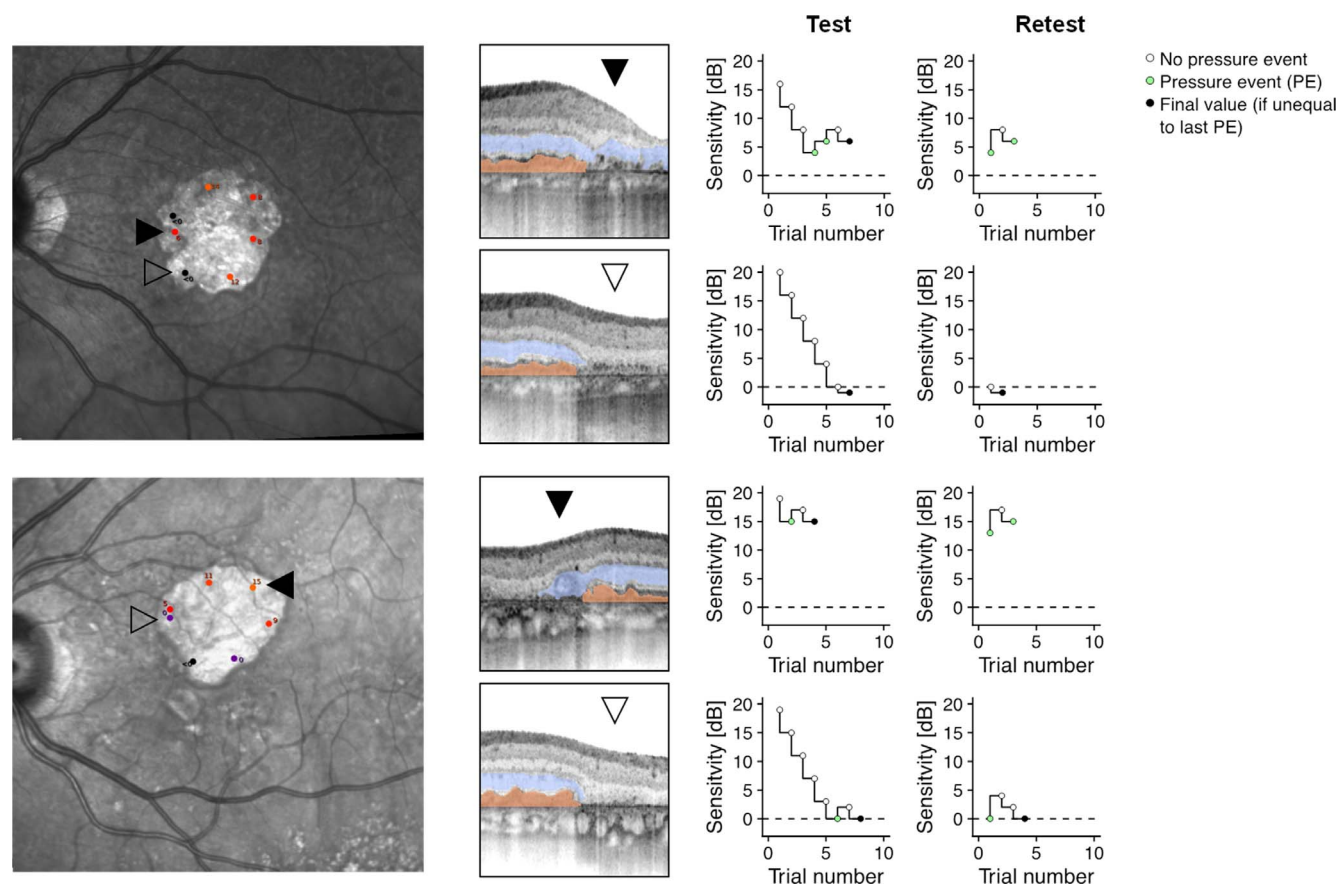


FIGURE 5. Exemplary patients. This figure shows the infrared reflection cSLO image with the superimposed results of the first mesopic FCP test (*left column*), the SD-OCT B-scan corresponding to the center of two exemplary stimuli (*central column*), and the results of the first and second mesopic FCP test for these two test points (*right column*) for two exemplary patients. The first test point of the first patient (*opaque arrowhead*) was located at an inner junctional zone with residual HFL+ONL (*blue overlay*). The first test shows that the patient responded to the 4-dB stimulus and 6-dB stimulus (indicated by the *green circles*), resulting in a final sensitivity of 6 dB, which was confirmed by the retest. The second test point for the first patient (*transparent arrowhead*) was located at an inner junctional zone with cRORA (complete atrophy of the RPE and outer retina). Accordingly, no function was measured during the test and retest. The second patient exhibited for the test point in proximity to the outer retinal tabulation (*opaque arrowhead*) sensitivity in the first test as well as the retest. This patient again shows no sensitivity for the stimulus located at the inner junctional zone with cRORA (*transparent arrowhead*).

of a 10- to 15-fold difference in retinal sensitivity across the boundary of RPE atrophy. Accordingly, even for the subset of regions with residual HFL+ONL within atrophic areas, the boundary of RPE atrophy would delineate approximately a 5-dB (i.e., three-fold) drop in sensitivity. Therefore, FAF is nevertheless a good surrogate of dysfunction, and can serve as structural end point in trials aiming to slow or halt the progression of GA.^{6,54} Secondly, clinical trials investigating therapeutic approaches for AMD requiring subretinal surgery (e.g., subretinal delivery of gene therapy, RPE, or photoreceptor cell replacement) need to be analyzed with great scrutiny. Any subretinal intervention may potentially to some degree relocate nonatrophic neuroretina to areas of RPE atrophy. In this scenario, a subsequent (transient) increase in sensitivity in this region of RPE atrophy would be expected based on the results shown here, independent of direct treatment effect. Localized measures of rod-mediated function (e.g., dark-adapted FCP) may constitute accordingly a much more meaningful outcome measure in the setting of RPE cell replacement trials to proof RPE cell survival and contribution to the canonical RPE visual cycle.

Several limitations of the study need to be considered. It represents a post hoc analysis of perimetry testing with a test strategy aiming toward refined characterization of the outer

junctional zone (i.e., nonatrophic side of the GA boundary). Accordingly, the amount of collected data for the inner junctional zone was limited. While the marked effect estimates are strongly indicative for remnant cone photoreceptors with partially preserved function in areas of residual ONL, conclusions for ORTs may not be drawn due to the limited number of test points colocalizing with ORTs. Also, the retest-variability for the threshold determinations in the setting of severe functional loss was rather high, as shown in Table 2. However, through duplicate testing, which was considered by the mixed-model analyses, the sampling variability for each test point was reduced. Moreover, residual hyperreflective spots internal to Bruch's membrane could be observed at times in conjunction with residual HFL+ONL (e.g., upper patient in Fig. 5). Based on histopathologic studies, these may reflect either isolated melanosome/lipofuscin granules or dissociated, migrated RPE cells.^{11,55} The herein used stimulus size (Goldmann III) for FCP did not allow for a meaningful differential analysis of the effect of these potential dissociated RPE cells on retinal sensitivity. Moreover, smaller stimuli (e.g., adaptive optics scanning laser ophthalmoscopy-based perimetry) might also allow reducing potential light scatter to neighboring regions. Last, light-adapted (e.g., 10 cd/m² white background) testing with a red stimulus would have further provided evidence that

the residual function measured was indeed cone mediated.²⁹ However, the S-MAIA device does not offer these test conditions as of now. Nevertheless, based on the analysis of the dark-adapted cyan-red sensitivity difference, the measured function was likely cone mediated.

In summary, this study demonstrates that the inner junctional zone of GA may constitute a deep, but yet not absolute scotoma using a highly conservative analysis with consideration of examination-specific (false-positive response rate, fixation stability, staircase strategy) and test point-specific factors (initial brightness) as well as the hierarchical structure of the data (test point nested in eye). The significant dependence of the measured sensitivity on the location-specific outer retinal configuration and the stimulus wavelength (i.e., photoreceptor class specificity) further support that residual cone-mediated function may be present within GA at the inner junctional zone.

Acknowledgments

The authors thank Verena Bonn, Joanna Czauderna, and Ruth Hassenrik for patient coordination and data acquisition.

Supported by the BONFOR Program of the Faculty of Medicine, University of Bonn, Grant No. O-137.0022 and O-137.0025 (MP); Novartis Pharma GmbH, EYEnovative Förderpreis 2017 (MP), and by the German Research Foundation (DFG), FL658/4-1 and FL658/4-2 (MF). CenterVue SpA (Padova, Italy) has provided research material (S-MAIA) for the conduct of this study. CenterVue had no role in the design or conduct of the experiments.

Disclosure: **M. Pfau**, Heidelberg Engineering (F), Optos (F), Carl Zeiss Meditec (F), CenterVue (F), Novartis (F); **L. von der Emde**, Heidelberg Engineering (F), Optos (F), Carl Zeiss Meditec (F), CenterVue (F); **C. Dysli**, Heidelberg Engineering (F), Optos (F), Carl Zeiss Meditec (F), CenterVue (F); **S. Thiele**, Heidelberg Engineering (F), Optos (F), Carl Zeiss Meditec (F), CenterVue (F); **P.T. Möller**, Heidelberg Engineering (F), Optos (F), Carl Zeiss Meditec (F), CenterVue (F); **M. Lindner**, Heidelberg Engineering (F), Optos (F), Carl Zeiss Meditec (F), CenterVue (F); **J. Nadal**, None; **M. Schmid**, None; **S. Schmitz-Valckenberg**, Heidelberg Engineering (F, R), Optos (F), Carl Zeiss Meditec (F), CenterVue (F), Allergan (F, R), Alcon/Novartis (F, R), Bioeq/Fermycon (F), Genentech/Roche (F, R), Bayer (F, R); **F.G. Holz**, Heidelberg Engineering (F, C, R), Optos (F), Carl Zeiss Meditec (F, C), CenterVue (F), Allergan (F, R), Alcon/Novartis (F, R), Genentech/Roche (F, R), Bayer (F, R), Acucela (F, R), Boehringer Ingelheim (F, R); **M. Fleckenstein**, Heidelberg Engineering (F, R), Optos (F), Carl Zeiss Meditec (F), CenterVue (F), Alcon/Novartis (F, R), Bayer (F, R), Alimera (F, R), P

References

- Cheung LK, Eaton A. Age-related macular degeneration. *Pharmacotherapy*. 2013;33:838-855.
- Holz FG, Schmitz-Valckenberg S, Fleckenstein M. Recent developments in the treatment of age-related macular degeneration. *J Clin Invest*. 2014;124:1430-1438.
- Rasmussen A, Sander B. Long-term longitudinal study of patients treated with ranibizumab for neovascular age-related macular degeneration. *Curr Opin Ophthalmol*. 2014;25:158-163.
- Schmitz-Valckenberg S. The journey of "geographic atrophy" through past, present, and future. *Ophthalmologica*. 2017; 237:11-20.
- Holz FG, Bindewald-Wittich A, Fleckenstein M, Dreyhaupt J, Scholl HP, Schmitz-Valckenberg S; FAM-Study Group. Progression of geographic atrophy and impact of fundus autofluorescence patterns in age-related macular degeneration. *Am J Ophthalmol*. 2007;143:463-472.
- Pfau M, Goerdt L, Schmitz-Valckenberg S, et al. Green-light autofluorescence versus combined blue-light autofluorescence and near-infrared reflectance imaging in geographic atrophy secondary to age-related macular degeneration. *Invest Ophthalmol Vis Sci*. 2017;58:BIO121-BIO130.
- Csaky KG, Richman EA, Ferris FL. Report from the NEI/FDA ophthalmic clinical trial design and endpoints symposium. *Invest Ophthalmol Vis Sci*. 2008;49:479-489.
- Fleckenstein M, Issa PC, Helb HM, et al. High-resolution spectral domain-OCT imaging in geographic atrophy associated with age-related macular degeneration. *Invest Ophthalmol Vis Sci*. 2008;49:4137-4144.
- Sarks SH. Ageing and degeneration in the macular region: a clinico-pathological study. *Br J Ophthalmol*. 1976;60:324-341.
- Zanzottera EC, Ach T, Huisinck C, Messinger JD, Spaide RF, Curcio CA. Visualizing retinal pigment epithelium phenotypes in the transition to geographic atrophy in age-related macular degeneration. *Retina*. 2016;36:S12-S25.
- Li M, Huisinck C, Messinger J, et al. Histology of geographic atrophy secondary to age-related macular degeneration: a multilayer approach. *Retina*. 2018;38:1937-1953.
- Staurengi G, Sadda S, Chakravarthy U, Spaide RF; International Nomenclature for Optical Coherence Tomography (IN•OCT) Panel. Proposed lexicon for anatomic landmarks in normal posterior segment spectral-domain optical coherence tomography: the IN•OCT consensus. *Ophthalmology*. 2014;121:1572-1578.
- Tan ACS, Astroz P, Dansingani KK, et al. The evolution of the plateau, an optical coherence tomography signature seen in geographic atrophy. *Invest Ophthalmol Vis Sci*. 2017;58: 2349-2358.
- Zanzottera EC, Ach T, Huisinck C, Messinger JD, Freund KB, Curcio CA. Visualizing retinal pigment epithelium phenotypes in the transition to atrophy in neovascular age-related macular degeneration. *Retina*. 2016;36:S26-S39.
- Bearely S, Chau FY, Koreishi A, Stinnett SS, Izatt JA, Toth CA. Spectral domain optical coherence tomography imaging of geographic atrophy margins. *Ophthalmology*. 2009;116: 1762-1769.
- Sadda SR, Guymer R, Holz FG, et al. Consensus definition for atrophy associated with age-related macular degeneration on OCT: Classification of Atrophy Report 3. *Ophthalmology*. 2018;125:537-548.
- Schaal KB, Freund KB, Litts KM, Zhang Y, Messinger JD, Curcio CA. Outer retinal tubulation in advanced age-related macular degeneration: optical coherence tomographic findings correspond to histology. *Retina*. 2015;35:1339-1350.
- Dolz-Marco R, Litts KM, Tan ACS, Freund KB, Curcio CA. The evolution of outer retinal tubulation, a neurodegeneration and gliosis prominent in macular diseases. *Ophthalmology*. 2017; 124:1353-1367.
- Lindner M, Böker A, Mauschitz MM, et al. Directional kinetics of geographic atrophy progression in age-related macular degeneration with foveal sparing. *Ophthalmology*. 2015;122: 1356-1365.
- Pfau M, Lindner M, Goerdt L, et al. Prognostic value of shape-descriptive factors for the progression of geographic atrophy secondary to age-related macular degeneration. *Retina*. 2019; 39:1527-1540.
- Pfau M, Müller PL, von der Emde L, et al. Mesopic and dark-adapted two-color fundus-controlled perimetry in geographic atrophy secondary to age-related macular degeneration [published online ahead of print October 8, 2018]. *Retina*. doi:10.1097/IAE.0000000000002337.
- Li M, Dolz-Marco R, Huisinck C, et al. Clinicopathologic correlation of geographic atrophy secondary to age-related macular degeneration. *Retina*. 2019;39:802-816.

23. Schmitz-Valckenberg S, Brinkmann CK, Alten F, et al. Semi-automated image processing method for identification and quantification of geographic atrophy in age-related macular degeneration. *Invest Ophthalmol Vis Sci*. 2011;52:7640-7646.
24. Pfau M, Lindner M, Fleckenstein M, et al. Test-retest reliability of scotopic and mesopic fundus-controlled perimetry using a modified MAIA (macular integrity assessment) in normal eyes. *Ophthalmologica*. 2017;237:42-54.
25. Pfau M, Lindner M, Muller PL, et al. Effective dynamic range and retest reliability of dark-adapted two-color fundus-controlled perimetry in patients with macular diseases. *Invest Ophthalmol Vis Sci*. 2017;58:BIO158-BIO167.
26. von der Emde L, Pfau M, Thiele S, et al. Mesopic and dark-adapted two-color fundus-controlled perimetry in choroidal neovascularization secondary to age-related macular degeneration. *Trans Vis Sci Tech*. 2019;8(1):7.
27. Jacobson SG, Voigt WJ, Parel J-M, et al. Automated light- and dark-adapted perimetry for evaluating retinitis pigmentosa. *Ophthalmology*. 1986;93:1604-1611.
28. Pfau M, Lindner M, Steinberg JS, et al. Visual field indices and patterns of visual field deficits in mesopic and dark-adapted two-colour fundus-controlled perimetry in macular diseases. *Br J Ophthalmol*. 2018;102:1054-1059.
29. Jacobson SG, Apáthy PP, Parel J-M. Rod and cone perimetry: computerized testing and analysis. In: Heckenlively JR, Arden GB, eds. *Principles and Practice of Clinical Electrophysiology of Vision*. St. Louis, MO: Mosby, Inc.; 1991:475-482. Available at: <http://www.iscecv.org/varia/ArdenHeckenlively1991Principles/Part%20XI%20Psychophysical%20Testing/60%20Rod%20and%20Cone%20Perimetry%20Computerized%20Testing%20and%20Analysis.pdf>
30. Bland JM, Altman DG. Measuring agreement in method comparison studies. *Stat Methods Med Res*. 1999;8:135-160.
31. Heijl A, Krakau CE. An automatic static perimeter, design and pilot study. *Acta Ophthalmol*. 1975;53:293-310.
32. Olsson J, Bengtsson B, Heijl A, Rootzen H. An improved method to estimate frequency of false positive answers in computerized perimetry. *Acta Ophthalmol Scand*. 1997;75:181-183.
33. Curcio C, Sloan K, Kalina R, Hendrickson A. Human photoreceptor topography. *J Comp Neurol*. 1990;4:497-523.
34. Sunness J, Johnson M, Massof R. Retinal sensitivity over drusen and nondrusen areas. A study using fundus perimetry. *Arch Ophthalmol*. 1988;106:1081-1084.
35. Schmitz-Valckenberg S, Bultmann S, Dreyhaupt J, Bindewald A, Holz FG, Rohrschneider K. Fundus autofluorescence and fundus perimetry in the junctional zone of geographic atrophy in patients with age-related macular degeneration. *Invest Ophthalmol Vis Sci*. 2004;45:4470-4476.
36. Meleth AD, Mettu P, Agrón E, et al. Changes in retinal sensitivity in geographic atrophy progression as measured by microperimetry. *Invest Ophthalmol Vis Sci*. 2011;52:1119-1126.
37. Chen FK, Patel PJ, Webster AR, Coffey PJ, Tufail A, Da Cruz L. Nidek MP1 is able to detect subtle decline in function in inherited and age-related atrophic macular disease with stable visual acuity. *Retina*. 2011;31:371-379.
38. Querques L, Querques G, Forte R, Souied EH. Microperimetric correlations of autofluorescence and optical coherence tomography imaging in dry age-related macular degeneration. *Am J Ophthalmol*. 2012;153:1110-1115.
39. Hariri AH, Tepelus TC, Akil H, Nittala MG, Sadda SR. Retinal sensitivity at the junctional zone of eyes with geographic atrophy due to age-related macular degeneration. *Am J Ophthalmol*. 2016;168:122-128.
40. Hartmann KI, Bartsch DU, Cheng L, et al. Scanning laser ophthalmoscope imaging stabilized microperimetry in dry age-related macular degeneration. *Retina*. 2011;31:1323-1331.
41. Takahashi A, Ooto S, Yamashiro K, et al. Photoreceptor damage and reduction of retinal sensitivity surrounding geographic atrophy in age-related macular degeneration. *Am J Ophthalmol*. 2016;168:260-268.
42. Pilotto E, Benetti E, Convento E, et al. Microperimetry, fundus autofluorescence, and retinal layer changes in progressing geographic atrophy. *Can J Ophthalmol*. 2013;48:386-393.
43. Sayegh R, Kiss C, Simader C, et al. A systematic correlation of morphology and function using spectral domain optical coherence tomography and microperimetry in patients with geographic atrophy. *Br J Ophthalmol*. 2014;98:1050-1055.
44. Wu Z, Ayton LN, Luu CD, Guymer RH. Microperimetry of nascent geographic atrophy in age-related macular degeneration. *Invest Ophthalmol Vis Sci*. 2015;56:115-121.
45. Wang J-S, Kefalov VJ. The cone-specific visual cycle. *Prog Retin Eye Res*. 2011;30:115-128.
46. Curcio CA, Medeiros NE, Millican CL. Photoreceptor loss in age-related macular degeneration. *Invest Ophthalmol Vis Sci*. 1996;37:1236-1249.
47. Curcio CA, Owsley C, Jackson GR. Spare the rods, save the cones in aging and age-related maculopathy. *Invest Ophthalmol Vis Sci*. 2000;41:2015-2018.
48. Sarks JP, Sarks SH, Killingsworth MC. Evolution of geographic atrophy of the retinal pigment epithelium. *Eye*. 1988;2:552-577.
49. Dysli C, Wolf S, Berezin MY, Sauer L, Hammer M, Zinkernagel MS. Fluorescence lifetime imaging ophthalmoscopy. *Prog Retin Eye Res*. 2017;60:120-143.
50. Dysli C, Wolf S, Zinkernagel MS. Autofluorescence lifetimes in geographic atrophy in patients with age-related macular degeneration. *Invest Ophthalmol Vis Sci*. 2016;57:2479.
51. Sauer L, Klemm M, Peters S, et al. Monitoring foveal sparing in geographic atrophy with fluorescence lifetime imaging ophthalmoscopy—a novel approach. *Acta Ophthalmol*. 2018;96:257-266.
52. Johnson PT, Lewis GP, Talaga KC, et al. Drusen-associated degeneration in the retina. *Invest Ophthalmol Vis Sci*. 2003;44:4481-4488.
53. Shelley EJ, Madigan MC, Natoli R, Penfold PL, Provis JM. Cone degeneration in aging and age-related macular degeneration. *Arch Ophthalmol*. 2009;127:483-492.
54. Holz FG, Sadda SR, Staurenghi G, et al. Imaging protocols in clinical studies in advanced age-related macular degeneration: recommendations from classification of atrophy consensus meetings. *Ophthalmology*. 2017;124:464-478.
55. Rudolf M, Vogt SD, Curcio CA, et al. Histologic basis of variations in retinal pigment epithelium autofluorescence in eyes with geographic atrophy. *Ophthalmology*. 2013;120:821-828.